IEEE Access
Multidisciplinary | Rapid Review | Open Access Journal

Received October 15, 2018, accepted October 23, 2018, date of publication November 9, 2018,
date of current version November 30, 2018.

Digital Object Identifier 10.1109/ACCESS.2018.2878818

Random Access Preamble Design for High-Velocity User in Millimeter-Wave Cellular Networks

MOHAMMED SAQUIB KHAN[1], ROTHNA PEC[1], CHANG HWAN PARK[2], AND YONG SOO CHO[1]
[1]Department of Electrical and Electronics Engineering, Chung-Ang University, Seoul 06974, South Korea
[2]LG Electronics, Seoul 06772, South Korea

Corresponding author: Yong Soo Cho (yscho@cau.ac.kr)

This work was supported by the National Research Foundation of Korea through the Korea Government under Grant MSIT 2018R1A2B2002621 and Grant 2018R1A4A1023826.

ABSTRACT In this paper, a design technique of random access preamble (RAP) for high-velocity users (HVUs) in millimeter-wave (mmWave) cellular networks is proposed. After demonstrating the inefficiency of the conventional long-term evolution (LTE)-based RAP for HVUs in mmWave networks, linear-frequency-modulation-based RAP (LFM RAP) is proposed for the detection of HVUs. The correlation of LTE-based RAP, and ambiguity and extended-ambiguity functions of LFM RAP are analyzed to examine their properties affected by the high-velocity of the user. The performance of RAPs is evaluated through detection and false alarm probabilities in a high-velocity and multiuser environment. The results show that the LFM RAP is appropriate for HVUs in mmWave cellular networks because of its high-detection probability in a high-speed environment.

INDEX TERMS Extended-ambiguity function, high-velocity user, LFM, millimeter-wave, random access preamble.

I. INTRODUCTION

Owing to the widespread use of smartphones for various applications and services, there has been a rapid increase in mobile data traffic. Millimeter-wave (mmWave) communication is an enabling technology that has countless applications. The abundant spectrum available at these high frequencies can deliver extreme data speeds and capacity required for future cellular communication networks. In addition, the technology is being considered for mobile broadband communications in 5G New Radio (5G NR) and 5G Special Interest Group (5G SIG), all of which are based on orthogonal frequency division multiplexing (OFDM) [1], [2].

Vehicle-to-vehicle (V2V), vehicle-to-infrastructure (V2I), or vehicle-to-everything (V2X) is one of the most important application areas where the NR can be applied. MmWave V2X communication networks are currently investigated because of their potential for gigabit-per-second data rate [3]. However, the OFDM-based mmWave V2X communication network is sensitive to Doppler frequency shift because of high-speed movement in a high-frequency band. MmWave V2X networks are particularly sensitive to Doppler shift in the initial access period because it cannot be compensated in this period.

The conventional LTE-based random access preamble (RAP), also known as Zadoff-Chu RAP (ZC RAP), can be considered for random access in mmWave V2X networks [4]. However, the ZC RAP may not be suitable for a high velocity user (HVU) in mmWave V2X networks because of its sensitivity to Doppler shift. To solve the issue of Doppler shift in high-mobility scenarios, numerous research work has been done in performance optimization of high-speed beamforming [5], [6], handover [7]–[9], and random access [10]–[13]. In these documents, the authors emphasize that the Doppler shift will cause the formation of the undesired-correlation peak (false peak) even when frequency error is lesser than one subcarrier spacing. Hence, the Doppler shift effect is severe in terms of the performance of both the detection and false-alarm probabilities. In [10]–[13], the authors have used the restricted sets of ZC sequence which is defined in the LTE specifications in order to generate the RAP. However, [5]–[13] considers the high-speed scenarios in LTE systems, where the carrier frequency is below 6 GHz. When compared to mmWave networks with a high carrier frequency, the LTE systems cause lower Doppler shifts. Hence, the upper bound of the Doppler shift in mmWave networks is underestimated by the

techniques proposed in these documents. In 3rd Generation Partnership Project 5th Generation New Radio (3GPP 5G NR) standard [14], a possible solution is adopted to overcome the effect of high Doppler shift for above-6GHz mmWave band by considering the higher subcarrier spacings (SCSs). This implies that the sensitivity of the ZC sequence to Doppler shift can be reduced by increasing the SCS. However, when the SCS is increased from {1.25, 5} kHz for below 6-GHz to {15, 30, 60, 120} kHz for above 6-GHz, the length of the sequence is reduced from 839 to 139. This in-turn reduces the number of available preambles [15]. Thus, NR long-preamble sequence (839) has a higher number of available preambles compared to the NR short-preamble sequence. In this paper, a different RAP based on linear frequency modulation (LFM) signal for HVU in mmWave V2X networks is investigated. To the best of the authors' knowledge, the LFM signal has so far not been used in cellular networks. However, the LFM signal has been widely used for the measurement of range and Doppler information in radar and sonar systems because of its insensitivity to Doppler shift [16]. In radar and sonar systems, the transmitted signal is correlated with the received echo signal to estimate the parameters such as range, angle, and velocity. In these systems, there is no need to carry the information of the transmitter identity in the transmitted signal. However, in cellular networks, a large number of RAPs need to be generated so that the BS can distinguish the different accessing MSs. In the conventional LTE system, a total of 64 different preambles are used.

In this study, a new RAP design technique for HVUs in mmWave V2X networks is proposed. First, the inaptness of the conventional ZC RAP for HVUs in mmWave V2X networks is presented. Next, to overcome the effect of Doppler and detection ambiguity, the LFM-based RAP (LFM RAP) is proposed. Utilizing a Doppler-shift insensitive LFM signal, the LFM RAP is created in which the preamble identification (PID) of the HVU is assigned to its frequency sweep and frequency shift parameters. Then, the ambiguity function (AF) of LFM RAP is analyzed to examine its correlation property under the influence of the Doppler shift and time shift. Subsequently, the extended-ambiguity function (EAF) is defined to examine the cross-correlation properties of the proposed LFM RAP with distinct IDs of HVU, under the influence of Doppler shift and time shift. Finally, the performance of RAPs is examined by evaluating the false-alarm and detection probabilities in Doppler environments.

II. RAP DESIGN

A. ZC RAP

In LTE, the RAP is generated by cyclically shifting the prime-length ZC sequence, where the root index of the sequence is unique to each cell. The cyclic shifts of the base sequence, which is of length 839, are used to generate 64 different preambles. An MS randomly selects one of the 64 available PIDs and transmits the RAP in the Physical Random Access Channel (PRACH) [4]. The u^{th} root ZC sequence of length is given as follows:

$$x_{ZC}^{u}(n) = e^{-j\frac{\pi un(n+1)}{N}}, \quad 0 \le n \le N-1 \tag{1}$$

From the u^{th} root ZC sequence that is assigned to each cell, the PIDs with a zero correlation zone (ZCZ) of length $(N_{\mathrm{CS}}-1)$ are defined by the cyclic shifts, C_v, as follows:

$$x_{ZC}^{u,v}(n) = x^{u}((n+C_v) \bmod N) \tag{2}$$

where

$$C_v = \begin{cases} vN_{\mathrm{CS}} & v = 0,1,\cdots,\lfloor N/N_{\mathrm{CS}} \rfloor - 1,\ N_{\mathrm{CS}} \neq 0 \\ 0 & N_{\mathrm{CS}} = 0 \end{cases} \tag{3}$$

In the presence of Doppler shift, f_D, the ZC sequence in (1) is distorted as follows:

$$x_{ZC}^{u}(n,\varepsilon) = x_{ZC}^{u}(n) \cdot e^{\frac{j2\pi\varepsilon n}{N}} = x^{u}(n-\tilde{u}) \cdot e^{\frac{j2\pi n}{N}(\varepsilon-1)} \cdot e^{j\phi_u} \tag{4}$$

where $\varepsilon = f_D T_{\mathrm{SEQ}}$. T_{SEQ} and ϕ_u denote the duration of RAP and constant phase shift, respectively. The Doppler shift as large as one PRACH subcarrier ($\pm$1.25kHz for LTE) results in a cyclic shift of $(vN_{\mathrm{CS}} \pm d_u) \bmod N$. Here, d_u is defined as

$$d_u = \begin{cases} \tilde{u} \bmod N & 0 \le \tilde{u} \bmod N < N/2 \\ N - \tilde{u} \bmod N & \text{otherwise} \end{cases} \tag{5}$$

where $\tilde{u}$ is the multiplicative inverse of u. The correlation function of ZC RAP is given in terms of Doppler shift and time shift as follows:

$$\begin{aligned} R_{ZC}^{u_1,u_2}(\varepsilon, i_d) &= \frac{1}{N}\sum_{n=0}^{N-1} x^{u_1}(n,(\varepsilon - i_d))\left[x^{u_2}(n)\right]^* \\ &= \frac{1}{N}\begin{cases} N\,\mathrm{sinc}(\varepsilon - i_d) & u_1 = u_2 \\ (x^{u_{12}}(\tilde{u}_{12}\varepsilon))^* \sum^{u_1,u_2} & u_1 \neq u_2,\ \varepsilon = \varepsilon_I \end{cases} \end{aligned} \tag{6}$$

where i_d denotes the index of the side peak that occurs at the position $(vN_{\mathrm{CS}} \pm d_u) \bmod N$ because of the Doppler shift. When i_d and ε are zero, and $u_1 = u_2$, the normalized magnitude is one. In addition, when the value of ε is much smaller than N, the correlation magnitude at the correct index can be approximated as $|R_x(\varepsilon, 0)| \approx \mathrm{sinc}(\varepsilon)$. At the correct index, the magnitude decreases with increase in Doppler shift. When $\varepsilon = \varepsilon_I$ (integer), the magnitude at the correct index becomes zero. When $u_1 \neq u_2$, the closed form solution cannot be obtained for all values of ε. However, when $\varepsilon = \varepsilon_I$, the cross-correlation function can be expressed as in (6). The term, $\left|\sum^{u_1,u_2}\right|$, in (6) is $\sqrt{N}$ using the Gauss sum property. Here, $u_{12}u_1 - u_2$. These results prove that the effect of Doppler shift is significant for ZC RAP. The magnitude of autocorrelation at the correct index decreases with the increase in side peak in the Doppler environment.

B. LFM RAP

A finite length continuous LFM signal with symbol duration, τ, for an HVU v is given as [16]

$$x_{LFM}^{u,v}(t) = e^{j\pi\left(2f_u t + \frac{\beta_v}{\tau}t^2\right)}, \quad 0 \le t \le \tau \tag{7}$$

where f_u and β_v are the frequency shift and frequency sweeping parameters, respectively. The PID of the HVU is assigned to these parameters of the LFM signal. In (7), the values of f_u and β_v are given as

$$\begin{aligned} -B \le \beta_v \le B \\ \frac{-B + |\beta_{v_{\max}}|}{2} \le f_u \le \frac{B - |\beta_{v_{\max}}|}{2} \end{aligned} \tag{8}$$

where B represents the operational bandwidth of the channel, $v \in \{0, 1, 2, \cdots, 63\}$ and $u \in \{0, 1, \cdots\}$. The AF of LFM RAP with the PID v is given as

$$\begin{aligned} A_{LFM}^{v}(t, f_D) &= \int_{-\infty}^{\infty} x_{LFM}^{u,v}(s)\left[x_{LFM}^{u,v}(s-t)\right]^* e^{j2\pi f_D s} ds \\ &= e^{j\pi(2f_u + f_D)t}\,\mathrm{sinc}\left(\beta_v t + f_D\tau\right)\rho_{LFM}(t) \end{aligned} \tag{9}$$

where $\rho_{LFM}(t) = 1 - |t|/\tau$. From (9), it can be observed that the magnitude of AF of the LFM signal varies with respect to τ, f_D, and β_v [16]. Whereas, f_u does not have any effect on the magnitude of AF. Furthermore, the EAF of LFM RAP with the PIDs v and v' is defined and analyzed as follows:

$$\begin{aligned} &A_{LFM}^{v,v'}(t, f_D) \\ &= \int_{-\infty}^{\infty} x_{LFM}^{u,v}(s)\left[x_{LFM}^{u',v'}(s-t)\right]^* e^{j2\pi f_D s} ds \\ &= e^{j\pi\left(2f_{u'}t - \frac{\beta_{v'}}{\tau}t^2\right)} \cdot e^{-j\pi\Delta\beta\tau\left(\frac{(\Delta f + f_D)\tau + \beta_{v'}t}{\Delta\beta\tau}\right)^2} \\ &\quad \cdot \left(\frac{C^{v,v'}(t, f_D)}{a^{v,v'}\tau} + jsgn(\Delta\beta)\frac{S^{v,v'}(t, f_D)}{a^{v,v'}\tau}\right) \end{aligned} \tag{10}$$

where

$$\begin{aligned} &0 \le t \le \tau,\ \Delta f = f_u - f_{u'},\ \Delta\beta = \beta_v - \beta_{v'},\ \Delta\beta \ne 0, \\ &S^{v,v'}(t, f_D) = S\left(a^{v,v'}s_0 + b^{v,v'}(t, f_D)\right) \\ &\qquad + S\left(a^{v,v'}s_t - b^{v,v'}(t, f_D)\right), \\ &C^{v,v'}(t, f_D) = C\left(a^{v,v'}s_0 + b^{v,v'}(t, f_D)\right) \\ &\qquad + C\left(a^{v,v'}s_t - b^{v,v'}(t, f_D)\right), \\ &s_t = \frac{\tau}{2} - |t|,\ a^{v,v'} = \sqrt{\frac{|\Delta\beta|\pi}{\tau}}, \\ &b^{v,v'}(t, f_D) = \sqrt{|\Delta\beta|\tau\pi}\left(\frac{(\Delta f + f_D)\tau + \beta_{v'}t}{\Delta\beta\tau}\right) \end{aligned} \tag{11}$$

Here, $sgn(\cdot)$ represent the signum function with the values $\{1, 0\}$ for positive, and zero values of β_v, respectively. In (10), Fresnel Integrals are used to derive EAF, where cosine and sine Fresnel Integrals are given as follows [17]:

$$C_n(t) = \int_0^t \cos\left(\frac{\pi s^2}{2}\right) ds,\ S_n(t) = \int_0^t \sin\left(\frac{\pi s^2}{2}\right) ds \tag{12}$$

When $\beta_v = \beta_{v'}$, the EAF of LFM RAP can be analyzed as

$$\begin{aligned} &A_{LFM}^{v,v'}(t, f_D) \\ &= e^{j\pi\left(2f_u t - \frac{\beta_v}{\tau}t^2\right)} \int_{-\infty}^{\infty} e^{j2\pi\left(\Delta f + \frac{\beta_v}{\tau}t + f_D\right)s} ds \\ &= e^{j\pi(f_u + \Delta f + f_D)t}\,\mathrm{sinc}\left(\Delta f\tau + f_D\tau + \beta_v t\right) \end{aligned} \tag{13}$$

Since (13) can be seen as a shifted sinc function, the peak value, $\tilde{\rho}_{LFM}^{v,v'}$, corresponding to the time shift, $t_S^{v,v'}$, can be expressed as follows:

$$\tilde{\rho}_{LFM}^{v,v'} = \rho_{LFM}\left(t_S^{v,v'}\right),\ t_S^{v,v'} = -\frac{\tau}{\beta_v}(\Delta f + f_D) \tag{14}$$

For a fixed value of β_v, the time shift will increase proportionally with respect to the values of $f_u, f_{u'}$, and f_D. Moreover, the value of the peak decreases with increase in the time shift. (14) indicates that the symbol duration should be smaller than the time shift in order to avoid false detection, i.e.,

$$\frac{\left|t_S^{v,v'}\right|}{\tau} \ge 1 \Leftrightarrow |\Delta f + f_D| \ge |\beta_v| \tag{15}$$

To avoid time ambiguity, the condition of Δf can be obtained from (8) and (15), such that f_D is far smaller than Δf, as follows:

$$\beta_v \le \Delta f \le \frac{B - \beta_v}{2}, \quad \beta_v > 0 \tag{16}$$

For all the values of β_v lesser than $B/3$, the condition in (16) is satisfied. When β_v is greater than $B/3$, the number of LFM RAPs that can be generated with β_v is one, otherwise, it can cause time ambiguity.

The value of $\Delta\beta$ should be precisely selected to secure a low correlation between RAPs whereas supporting a substantial number of RAPs. Using the LFM signal, the number of possible RAPs generated can be determined using the upper bound (UB) of EAF of the LFM RAP and is derived as follows:

$$\Gamma(\tau, \Delta\beta) = 2\sqrt{\frac{C_{\max}^2 + S_{\max}^2}{\Delta\beta\tau\pi}}, \quad \Delta\beta > 0 \tag{17}$$

where $S_{\max}$ and $C_{\max}$ denote the maximum values of sine and cosine Fresnel integrals, respectively. The non-normalized values of $S_{\max}$ and $C_{\max}$ can be obtained by using s^2 in (12) as 0.8948 and 0.9775, respectively. From (17), it can be seen that the UB values are independent of the frequency shift, f_u and Doppler shift, f_D, thus showing no significant effect of f_u and f_D on the EAF. The separation value, $\Delta\beta$, between β_v and $\beta_{v'}$ and the symbol duration, τ, are critical. The value of $\Delta\beta\tau$ is inversely proportional to the value of the UB.

III. RAP DETECTION

When the ZC or LFM RAP is received from multiple HVUs in the same cell, the received signal at the serving BS, c, with the b^{th} Rx beam in the time domain is given as follows:

$$y_b^c(n) = \sum_{u=0}^{N_U-1}\sum_{m=0}^{N_M-1} G_{Tx,i}^{u,m} G_{Rx,b} h_{i,b}^{u,m}(n)\, x_{ZC/LFM}^{u,m}(n) + z(n) \tag{18}$$

where $G_{Tx,i}^{u,m}$, $G_{Rx,b}$, $h_{i,b}^{u,m}(n)$, $x_{ZC/LFM}^{u,m}(n)$, and $z(n)$ denotes the Tx beam gain at the i^{th} beam of the m^{th} HVU in the u^{th} cell, Rx beam gain at the b^{th} beam of BS, the channel impulse response between the i^{th} beam of the m^{th} HVU in the u^{th} cell and the b^{th} beam of the serving BS, $c \in u$, the ZC or LFM RAP transmitted from the m^{th} HVU in the u^{th} cell, and additive white Gaussian noise (AWGN), respectively. Also, N_U, N_M, N_I, and N_B denote the number of cells, the number of HVUs, the number of Tx beams, and the number of Rx beams, respectively.

For the detection of ZC RAP, the conventional technique described in [4] can be used. For the detection of LFM RAP, a detector consist of a set of correlators is used that match/correlate the received signal in parallel with a set of local LFM RAPs. The received signal at the input of the correlator for the detection of ZC RAP and at the input of the set of correlators for the detection of LFM RAP, respectively, are given as

$$y_{b,ZC/LFM}^{c}(n) = \begin{cases} \tilde{z}(n): & H_{ZC/LFM}^{0} \\ G_{Tx,i}^{c,0} G_{Rx,b} h_{i,b}^{c,0}(n)\, x_{ZC/LFM}^{c,0}(n) & \\ \quad +\tilde{z}(n): & H_{ZC/LFM}^{1} \end{cases} \tag{19}$$

where $x_{ZC/LFM}^{c,0}(n)$ denotes the desired signal and $\tilde{z}(n)$ denotes the interference from other HVUs and AWGN $z(n)$. The hypothesis H^0 refers to a case where all the undesired RAPs transmitted by $N_M - 1$ HVUs except HVU v is received as a received signal along with the noise. The hypothesis H^1 refers to a case where the RAP from the desired HVU v along with undesired RAPs is received as a received signal. The RAP is detected by computing the power-delay profile (PDP) of the received signal with a specific Tx beam and the output of the correlators is given as follows:

$$\left|r_b^{c,v}(s)\right|^2 = \left|\sum_{n=0}^{N-1} y_b^c(n) \left[x_{ZC/LFM}^{c,v}(n+s)\right]^*\right|^2 \tag{20}$$

where $r_b^{c,v}(s)$ denotes the correlation function between the received signal $y_b^c(n)$ and the reference ZC or LFM RAP, $x_{ZC}^{c,v}(n)$ or $x_{LFM}^{c,v}(n)$, respectively, with time lag s. From (20), the PDP peaks above the absolute detection threshold (γ) are searched over a search window corresponding to the cell size. The PID and timing advance (TA) is computed according to the position of the PDP peak, (I_{peak}), when ZC RAP is used, as follows:

$$PID_{ZC} = \left\lfloor I_{peak}/N_{\mathrm{CS}} \right\rfloor + 1; \quad TA_{ZC} = \mathrm{mod}(I_{peak}, N_{\mathrm{CS}}) - 1 \tag{21}$$

The desired LFM RAP and corresponding TA are detected from the PDP peaks obtained from the bank of the LFM RAP correlators as follows:

$$[PID_{LFM}, TA_{LFM}] = \arg\max_{b \in N_B} \left[\arg\max_{s} \left|r_b^{c,v}(s)\right|^2 > \gamma\right] \tag{22}$$

The performance of the RAP is evaluated through detection and false alarm probabilities [18]. The RAP detection probability depends on the detection threshold, which is determined by the false alarm probability. Under H^0, the PDP of the received signal will follow the central chi-square (χ^2) distribution with two degrees of freedom with a mean given by the noise floor level (λ_n), and then the false alarm probability can be obtained as

$$P_{FA} = P\left\{\max\left|r_b^{c,v}(s)\right|^2 > \gamma_{tr}\right\} = \left(1 - F_{r[H_0]}\{\gamma_{tr}\}\right)^{N_M} \tag{23}$$

where $\gamma_{tr}(=\gamma/\lambda_n)$ and F_r denote the threshold relative to λ_n and the cumulative distribution function of $\left|r_b^{c,v}(s)\right|^2$ under H^0 at γ_{tr}, respectively. F_r can be obtained as follows:

$$F_r = \left(1 - e^{-\gamma_{tr}} \sum_{b=0}^{N_B-1} \frac{1}{b!} (\gamma_{tr})^b\right)^N \tag{24}$$

Under H^1, the PDP of the received signal will follow the non-central chi-square ($\tilde{\chi}^2$) distribution. Then, the detection probability can be obtained by using the detection threshold as follows:

$$P_D = P\left\{\max\left|r_b^{c,v}(s)\right|^2 > \gamma\right\} = Q\left(\sqrt{\zeta}, \sqrt{\gamma}\right) \tag{25}$$

where $Q(\cdot)$ and ζ represent the Marcum Q-function and the non-centrality parameter, respectively.

IV. SIMULATION

In this section, the performance of ZC and LFM RAPs is evaluated via computer simulations using a simple model of a mmWave cellular network. For the simulation, the parameters such as subcarrier spacing, carrier frequency, fast Fourier transform (FFT) size, and the sequence length are set to 15 kHz, 28 GHz, 2048, and 839, respectively. A uniform linear array (ULA) configuration with eight antenna elements is considered at both the BS and HVU, and the parameters corresponding to the number of beams at HVU and BS are set as $N_I = N_B = 8$. A Rician fading channel is assumed between the BS and the HVUs. For simulation, the spatial channel model (SCM) is used with a k-factor of 10 dB and the number of rays in the non-line-of-sight (NLoS) path is set to 20 [19]. In this paper, it is assumed that the Tx and Rx beams are aligned and formed in the direction of a line-of- sight (LoS) path.

Fig. 1 shows the normalized autocorrelation function of ZC RAP (with root index $u = 660$, length of ZCZ $N_{\mathrm{CS}} = 13$, and PID $v = 43$) as a function of the Doppler shift. It shows the performance of the autocorrelation function assessed at three different position indices, $i_d = \{-1, 0, 1\}$, with the variation of the Doppler shift, as given in (6). It can be seen that $\left|R_{ZC}^{660,660}(\varepsilon, 0)\right|$ and $\left|R_{ZC}^{660,660}(\varepsilon, \pm 1)\right|$ follows a sinc function. The magnitude of $\left|R_{ZC}^{660,660}(0, 0)\right|$ is 1 and decreases with an increase in ε. The maximum values of $\left|R_{ZC}^{660,660}(\varepsilon, \pm 1)\right|$ occurs at the first nulling points

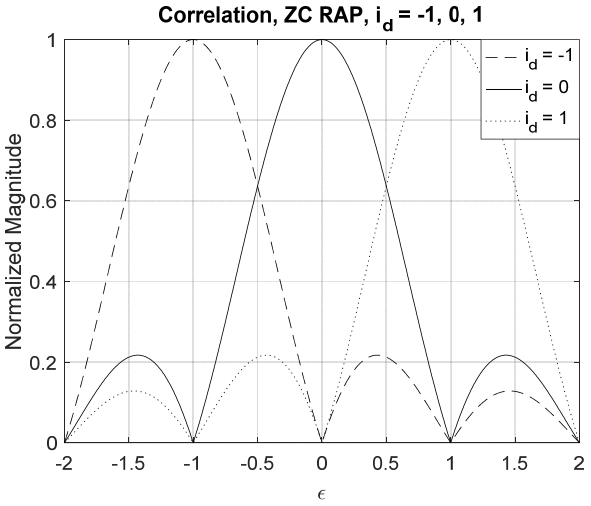

FIGURE 1. Autocorrelation function of ZC RAP vs. Doppler shift.

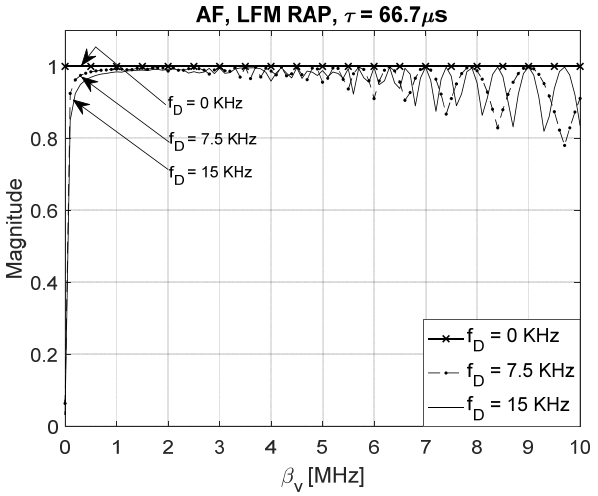

FIGURE 2. Effect of Doppler shift on AF of LFM RAP with varying β_v.

of $\left|R_{ZC}^{660,660}(\varepsilon,0)\right|$, i.e., at $\varepsilon = \pm 1$ ($f_D = \pm 15$ KHz). These results prove that the ZC RAP is very sensitive to Doppler shift. For example, when $f_D = 15$ kHz, the magnitude of the autocorrelation value of the desired peak becomes zero and the peak occurs at a different position ($i_d = 1$).

Next, the effect of f_D and β_v on the AF of LFM RAP in (9) is analyzed. The symbol duration is set to 66.7 μs. Fig. 2 shows the maximum magnitude of AF in the β_v domain for Doppler shifts, $f_D = \{0,\ 7.5,\ 15\}$kHz. When $f_D = 0 \mathrm{f_D} = 0$, it can be seen that the maximum magnitudes for all values of β_v are 1. However, the magnitude varies when the Doppler shift exists. It can be observed that when the value of β_v is small, the variation is severe. At $f_D = 15\mathrm{f_D}$= 15KHzkHz, the magnitude at $\beta_v = 0$ MHz becomes almost zero. A high detection probability of LFM RAP is obtained, when the value of β_v is selected to achieve a high magnitude of AF. From this figure, the smallest value of β_v is selected as 0.5 MHz and is used in further simulations.

Fig. 3 shows the comparative analytic and simulation results for EAF when f_D is zero, as given in (10) and (13). Fig. 3(a) shows the linear shift auto-correlation and EAF of two LFM RAPs generated with same frequency sweeping parameters, i.e., $\beta_v = \beta_{v'} = 0.5$ MHz, for cases where $f_u = f_{u'}$ and $f_u \neq f_{u'}$. Here, the normalized magnitude of EAF with $\beta_v = \beta_{v'}$ and $f_u = f_{u'}$ is one and comparatively same as that of ZC autocorrelation. Fig. 3(b) shows the linear-shift cross-correlation and EAF of two LFM RAPs when $\beta_v \neq \beta_{v'}$ ($\{\beta_v, \beta_{v'}\} = \{0.5,\ 0.6\}$ MHz), for cases where $f_u = f_{u'}$ and $f_u \neq f_{u'}$. The normalized value of EAF goes on decreasing with the increase of $\Delta\beta$ which is shown in Fig. 3(c). In Fig. 3(a) and 3(b), when $f_u \neq f_{u'}$, the magnitude of the peak is reduced, and the time shift occurs. From these results, it can be confirmed that analytic solutions given in (10) and (13) are well matched with the simulation results. Fig. 3(c) shows the EAF of LFM RAPs with $\beta_v = 0.5$ MHz and three different values of $\beta_{v'}$ (0.6 MHz, 5 MHz, 10 MHz), as given in (10). It can be seen that the magnitude of EAF decreases with the increase in $\Delta\beta$. This implies that when the value of $\Delta\beta$ increases, the cross-correlation of LFM RAPs becomes comparatively similar to that of ZC sequence.

Fig. 4 compares the analytic UB derived in (17) and the maximum value of EAF of LFM RAP obtained by simulations. In addition, β_0 denotes the minimum value

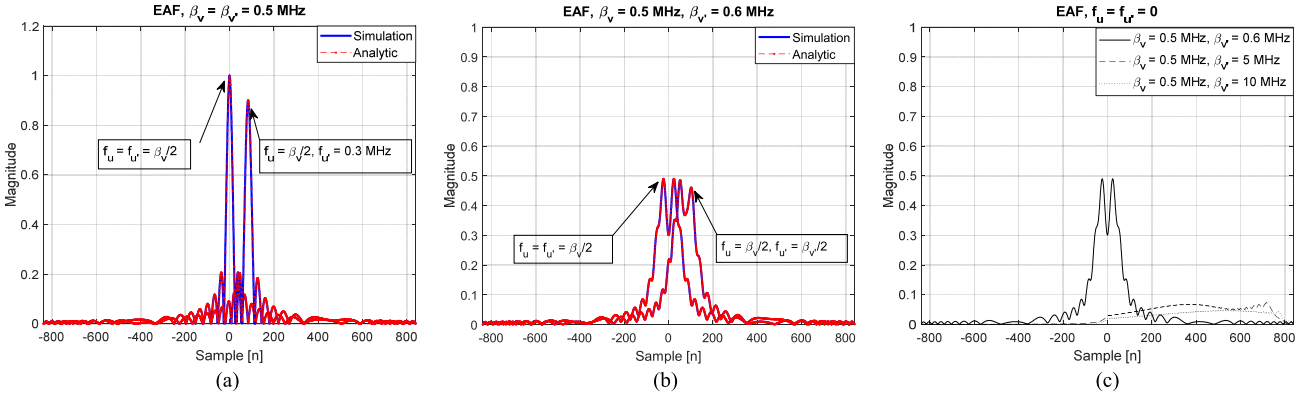

FIGURE 3. EAF of LFM RAP. (a) $\beta_v = \beta_{v'}$. (b) $\beta_v \neq \beta_{v'}$. (c) $\beta_v \neq \beta_{v'}$, $f_u = f_{u'} = 0$.

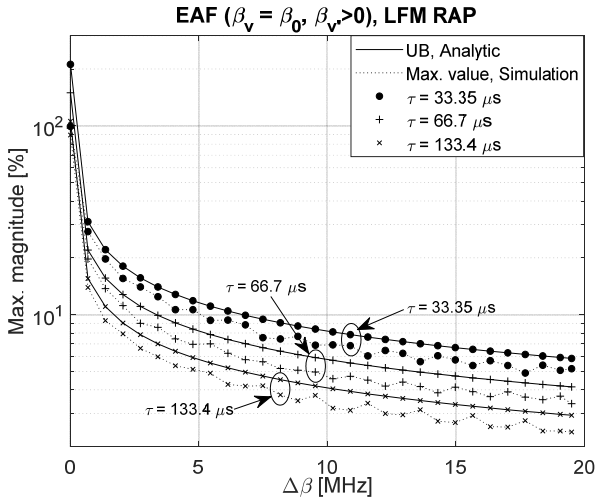

FIGURE 4. Upper bound and maximum EAF of LFM RAP.

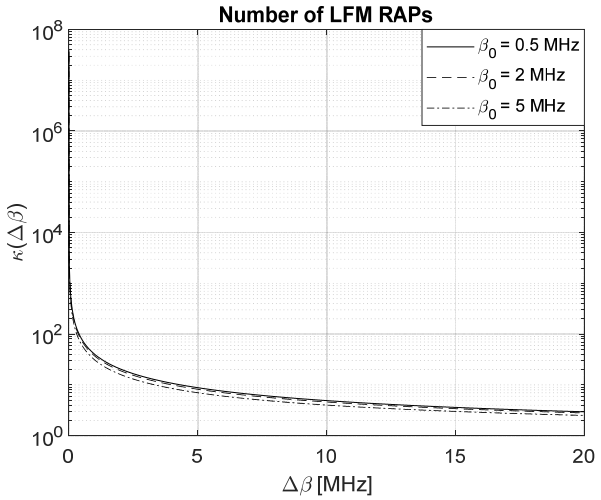

FIGURE 5. Possible number of LFM RAPs.

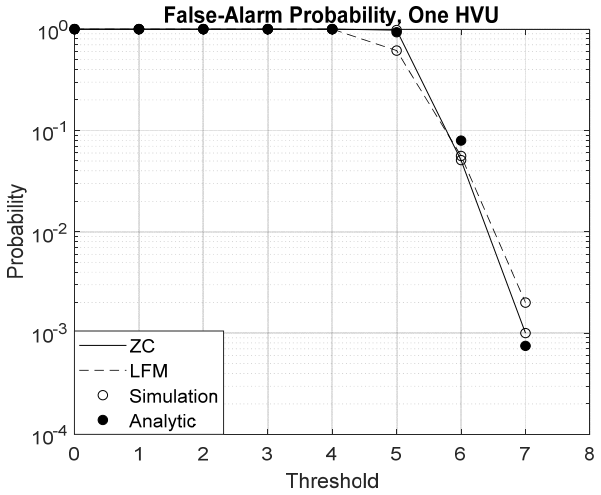

FIGURE 6. False alarm probability of ZC and LFM RAPs.

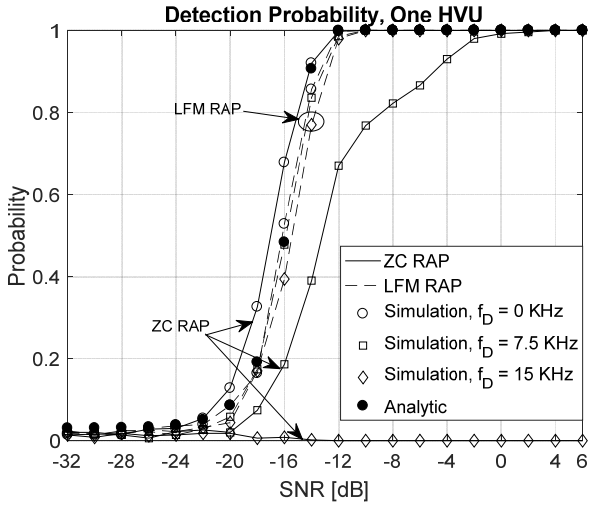

FIGURE 7. Detection probability of ZC and LFM RAPs.

of β_v (0.5 MHz). Also, $\beta_{v'}$ ($\beta_v + \Delta\beta$) is determined by varying the value of $\Delta\beta$. It can be seen from the figure that the UB value and the maximum value of EAF decreases with an increase in $\Delta\beta$ and τ. The simulation results are slightly lower than the analytic UBs.

Fig. 5 shows the possible number of LFM RAPs obtained from (17) by varying the value of $\Delta\beta$ for three different values of β_0. It can be seen that the value of $\Delta\beta$ is inversely proportional to the possible number of RAPs. Therefore, in the design of LFM RAP, there is a trade-off between the number of RAPs and the cross-correlation level with the selection of $\Delta\beta$. In addition, the possible number of RAPs obtained is the case considering only $\Delta\beta$ and can be increased when f_u is also considered. By considering $\Delta f = \beta_v < B/3$ in (17), with the same value of β_0 (0.5 MHz), the number of possible RAPs can be increased, and 38 additional RAPs can be obtained. The first 26 RAPs are achieved with $\beta_v = 0.5$ MHz and $|f_u| = \{0.5,\ 1,\ 1.5,\ \ldots, 6.5\}$ MHz and the remaining 12 RAPs are achieved with $\beta_v = 1$ MHz and $|f_u| = \{1,\ 2,\ \ldots,\ 6\}$ MHz.

Next, the false-alarm probabilities are obtained by the simulation and the analytic solution with zero Doppler shift given in (23). Fig. 6 shows the false-alarm probabilities of ZC and LFM RAPs when the number of HVUs, N_M, is one. This figure is obtained by setting the SNR to -30 dB and varying the threshold value, γ_{tr}, from 0 to 8. The value of the false-alarm probability is set to be less than or equal to 0.1% as in LTE systems [18]. From Fig. 6, it can be seen that the simulation is of good agreement with the analytic solution and a detection threshold equal to 7 can be selected for both ZC and LFM RAPs. This implies that the false-alarm probability of LFM RAP is similar to that of ZC RAP. This detection threshold value will be used to determine the detection probability. The detection threshold depends on the number of HVUs and increases with respect to the HVUs.

Fig. 7. shows the detection probabilities of ZC and LFM RAPs. The distance between the BS and HVU is set to 100 m. It is shown in the figure that the probability of detection of ZC RAP decreases with increase in Doppler shift. When f_D is zero, the detection probability reaches 100% at an

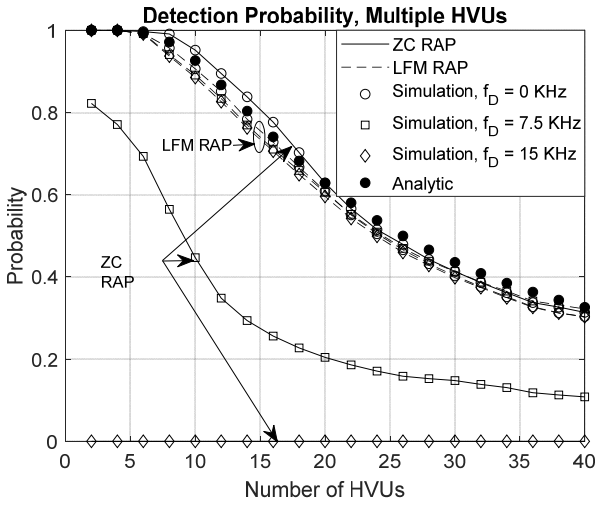

FIGURE 8. Detection probability of ZC and LFM RAPs when multiple HVUs exist.

TABLE 1. Property comparison of LFM and ZC RAPs.

Property	LFM	ZC
Sensitivity to Doppler	Insensitive	More insensitive as subcarrier spacing increases
Number of IDs	Larger as $\Delta\beta$ increases	Smaller as sequence length-N decreases
Cyclic Auto-correlation	Better as β_v increases	Ideal
Cross-correlation	Better as $\Delta\beta$ increases	Good
Favorable to	Linear shift correlation	Cyclic shift correlation

SNR of -12 dB, but when it is increased to 15 kHz, the detection probability becomes zero at all SNR regions. However, the detection probabilities of LFM RAP reaches 100% at SNRs of -12 and -10 dB when f_D is 0 and {7.5, 15} kHz, respectively.

The detection probability obtained through the analytic solution in (25) with zero Doppler shift is of good agreement with the simulation results for both RAPs with zero Doppler. The detection probability when multiple HVUs exist is shown in Fig. 8. For LFM RAP, the value of β_v is selected between 0.5 and 15 MHz with a step size, $\Delta\beta$, of 70 kHz. The detection probability for multiple HVUs ranging from 2 to 40 is obtained at an SNR of -8 dB and compared with the analytic solution given in (25). In the figure, it is shown that the detection probability decreases with an increase in the number of HVUs. When the number of HVUs, N_M, is 10, the detection probability of ZC RAP reduces to 95%, 45%, and 0% with Doppler shift values of 0, 7.5 and 15 kHz, respectively. That is, the detection probability of ZC RAP reduces significantly as the Doppler shift increases. However, the detection probability of LFM RAP is almost the same (similar to the analytic solution) regardless of the Doppler shift effect.

Finally, the properties of LFM and ZC RAPs are compared in Table I. In terms of peak to average power ratio (PAPR), both LFM and ZC RAPs have the same characteristic with constant envelops.

V. CONCLUSION

In this paper, it is shown that the ZC RAP has desirable properties in the absence of Doppler shift. However, it tends to deteriorate in the presence of Doppler shift, resulting in misdetection and time ambiguity. The EAF of LFM RAP is analyzed to examine the properties of LFM RAP with different HVU IDs under the influence of the Doppler shift, enabling the conditions for avoiding false detection and time ambiguity to be derived. In addition, the analytical solution for the upper bound of the cross-correlation level is provided. This can be used to select the suitable values of β_v and $\Delta\beta$ that are essential for the design of LFM RAPs. The LFM RAP is shown to be suitable for HVUs in mmWave cellular networks because of its high detection probability in a Doppler environment.

REFERENCES

[1] *Technical Specification Group Radio Access Network; NR; Physical Layer Procedures for Control (Release 15)*, document 3GPP TS 38.213 V 15.2.0, 3rd Gener. Partnership Project, Jun. 2018.

[2] *KT PyeongChang 5G Special Interest Group (KT 5G-SIG), KT 5th Generation Radio Access; Physical Layer; Physical Layer Procedures (Release 1)*, document TS 5G.213 V 1.9, KT, Sep. 2016.

[3] K. Lee, J. Kim, Y. Park, H. Wang, and D. Hong, "Latency of cellular-based V2X: Perspectives on TTI-proportional latency and TTI-independent latency," *IEEE Access*, vol. 5, pp. 15800–15809, 2017.

[4] S. Sesia, I. Toufik, and M. Baker, *LTE—The UMTS Long Term Evolution: From Theory to Practice*. Chichester, U.K.: Wiley, 2011.

[5] X. Chen, J. Lu, T. Li, P. Fan, and K. B. Letaief, "Directivity-beamwidth tradeoff of massive MIMO uplink beamforming for high speed train communication," *IEEE Access*, vol. 5, pp. 5936–5946, 2017.

[6] X. Liu and D. Qiao, "Location-fair beamforming for high speed railway communication systems," *IEEE Access*, vol. 6, pp. 28632–28642, 2018.

[7] O. B. Karimi, J. Liu, and C. Wang, "Seamless wireless connectivity for multimedia services in high speed trains," *IEEE J. Sel. Areas Commun.*, vol. 30, no. 4, pp. 729–739, May 2012.

[8] A. Parichehreh, U. Spagnolini, P. Marini, and A. Fontana, "Load-stress test of massive handovers for LTE two-hop architecture in high-speed trains," *IEEE Commun. Mag.*, vol. 55, no. 3, pp. 170–177, Mar. 2017.

[9] M. Cheng, X. Fang, and W. Luo, "Beamforming and positioning-assisted handover scheme for long-term evolution system in high-speed railway," *IET Commun.*, vol. 6, no. 15, pp. 2335–2340, Oct. 2012.

[10] D. Micheli *et al.*, "Over-the-air tests of high-speed moving LTE users in a reverberation chamber," *IEEE Trans. Veh. Technol.*, vol. 67, no. 5, pp. 4340–4349, May 2018.

[11] *Frequency Offset Effects on RACH Preamble Detectors*, document 3GPP TSG RAN WG1 Meeting #47, R1-063161, LG Electronics, Riga, Latvia, Nov. 2006.

[12] *Restricted Sets of RACH Preamble Signature for Environments With High Doppler Frequency Shifts*, document 3GPP TSG RAN WG1 #49, R1-070377, Nokia, Jan. 2007.

[13] *Using Restricted Preamble Set for RACH in High Mobility Environments*, document 3GPP TSG RAN WG1 #49, R1-073112, Samsung, Jun. 2007.

[14] *Technical Specification Group Radio Access Network; NR; Physical Channels and Modulation (Release 15)*, document 3GPP, TS 38.211-V15.2.0, 3rd Gener. Partnership Project, Jun. 2018.

[15] F. Khan, *LTE for 4G Mobile Broadband: Air Interface Technologies and Performance*. Cambridge, U.K.: Cambridge Univ. Press, 2009, pp. 238–240.

[16] M. A. Richards, *Fundamentals of Radar Signal Processing*, 2nd ed. New York, NY, USA: McGraw-Hill, 2015.

[17] I. S. Gradshteyn and I. M. Ryzhik, *Table of Integrals, Series, and Products*, 7th ed. Amsterdam, The Netherlands: Elsevier, 2007.

[18] D. A. Shnidman, "The calculation of the probability of detection and the generalized Marcum Q-function," *IEEE Trans. Inf. Theory*, vol. 35, no. 2, pp. 389–400, Mar. 1989.
[19] T. S. Rappaport *et al.*, "Millimeter wave mobile communications for 5G cellular: It will work!" *IEEE Access*, vol. 1, pp. 335–349, May 2013.

MOHAMMED SAQUIB KHAN was born in Mumbai, Maharashtra, India, in 1994. He received the B.E. degree in electronics and telecommunication engineering from the University of Mumbai, Mumbai, in 2015, and the M.S. degree in electrical and electronics engineering from Chung-Ang University, Seoul, South Korea, in 2017, where he is currently pursuing the Ph.D. degree in electrical and electronics engineering.

Since 2015, he has been a Research Assistant with Mobile Communications Lab, Chung-Ang University, Seoul, under the supervision of Dr. Cho. He has authored more than 15 international conferences and articles. His research interests include the areas of wireless communication systems and digital signal processing.

He is a member of the Korea Institute of Communications and Information Sciences.

ROTHNA PEC was born in Phnom Penh, Pursat, Cambodia, in 1988. He received the B.S. degree in electrical and electronics engineering from the Institute of Technology of Cambodia (ITC), Cambodia, in 2011, and the M.S. and Ph.D. degrees in electrical and electronics engineering from Chung-Ang University, Seoul, South Korea, in 2013 and 2017, respectively.

From 2011 to 2018, he was a Research Assistant with the Mobile Communications Lab, Chung-Ang University, under the supervision of Dr. Cho. Since 2018,he has been a Lecturer and a Researcher at ITC. He has authored more than 20 international conferences and articles.His research interests include beamforming, synchronization, and 5G.

CHANG HWAN PARK was born in Busan, South Korea, in 1982. He received the B.S., M.S., and Ph.D. degrees in electrical and electronics engineering from Chung-Ang University, Seoul, South Korea, in 2005, 2007, and 2011, respectively.

From 2005 to 2011, he was a Research Assistant with the Mobile Communications Lab, Chung-Ang University, under the supervision of Dr. Cho. Since 2011, he has been a Deputy Principal Research Engineer with LG Electronics, Seoul, where he has been involved in the standardization activities of LTE and 5G NR in 3GPP and developing a multi-modem chipset for HSPA+, LTE-A, and 5G. He has authored more than 50 conferences and articles. His research interests include the areas of mobile communication and digital signal processing, especially for MIMO-OFDM and 5G.

YONG SOO CHO was born in Seoul, South Korea. He received the B.S. degree in electronics engineering from Chung-Ang University, Seoul, South Korea, in 1984, the M.S. degree in electronics engineering from Yonsei University, Seoul, in 1987, and the Ph.D. degree in electrical and computer engineering from The University of Texas at Austin, Austin, TX, USA, in 1991.

He was a Research Engineer with Goldstar Electrical Company, Osan, South Korea, in 1984. He was a Visiting Research Fellow at the Electronics and Telecommunications Research Institute in 2001. Since 1992, he has been a Professor with the School of Electrical and Electronics Engineering, Chung-Ang University. He has authored twelve book and more than 400 conferences and articles. He holds more than 120 patents. His research interests include the areas of mobile communication and digital signal processing, especially for MIMO-OFDM and 5G.

Dr. Cho was the President of the Korean Institute of Communications and Information Sciences in 2016. He was a recipient of the Dr. Irwin Jacobs Award in 2013.